International Journal of Mechanical Sciences 131–132 (2017) 171–178

Contents lists available at ScienceDirect

International Journal of Mechanical Sciences

journal homepage: www.elsevier.com/locate/ijmecsci

Understanding the strength of bioinspired soft composites

Viacheslav Slesarenko [a], Konstantin Y. Volokh [b,*], Jacob Aboudi [c], Stephan Rudykh [a]

[a] Faculty of Aerospace Engineering, Technion – I.I.T., Israel
[b] Faculty of Civil and Environmental Engineering, Technion – I.I.T., Israel
[c] Faculty of Engineering, Tel Aviv University, Israel

A B S T R A C T

Remarkable mechanical properties of biocomposites (bone, teeth, shell, antler etc.) are usually attributed to their special design where staggered mineral platelets are embedded in a protein matrix. Because of the high aspect ratio of the platelet the soft protein deforms in the shear mode predominantly providing the linkage for the hard inclusions. Mimicking Nature one might design materials with a similar architecture.

By employing a micromechanical analysis, we study in the present work the strength of a bio-inspired composite in which hard platelets are embedded in a soft matrix made of the vulcanized natural rubber. We perform simulations of uniaxial tension of the composite material based on a continuum mechanics formulation and the high-fidelity generalized method of cells. The use of the energy limiters in the constitutive model for rubber at finite strains allows us to model failure and arrive at the overall strength of the composite.

We find that the overall strength of the composite depends on the deformation and failure of soft matrix in tension and shear. Moreover, we find that the strength of the composite cannot exceed the strength of the matrix. The latter observation is noteworthy because it is qualitatively different from the previous experimental results with biocomposites which show a dramatic (ten times) increase of the strength of the material as compared to the strengths of its constituents. We illustrate these analytical and numerical findings by our experiments on 3D printed composite materials.

1. Introduction

Natural biocomposites - bone, teeth, shell, antler etc. - exhibit high stiffness, strength, and fracture toughness. These mechanical properties are remarkable in view of the constituents that comprise biocomposites: *soft* protein or collagen matrix and *hard* mineral inclusions. The enigma of the mechanical behavior of biocomposites attracted many researchers: [3–6,9–12,14–17,26] to list a few.

It is clear today that the high stiffness of biocomposites is due to the very high percentage - 90% and more - of the stiff mineral constituent. Moreover, [11] suggest that “large aspect ratios and a staggered alignment of mineral platelets are found to be the key factors contributing to the large stiffness of biomaterials.” The latter architecture might also give qualitative insights into the high fracture toughness [11].

Nevertheless, the reason for the high strength of biocomposites is not clear. The increase of the strength of biocomposite as compared to the strength of its constituents is truly impressive. Indeed, the strength of shell protein and mineral separately are estimated as 20 MPa and 300 MPa respectively, while the shell overall strength is 100–300 MPa [9,12,14] the strength of bone collagen and mineral separately are estimated as 20 MPa and 300 MPa respectively, while the bone overall strength is 100 MPa [10,15]. Thus, the biocomposites have overall strength 10 times greater than the strength of soft matrix.

Is the biocomposite strength due it its architecture? If yes, then man-made composites with similar architecture can be produced [25]. For example, it is possible to create soft composites on the basis of rubberlike matrix enhanced with the staggered hard platelets of high (10 and more) aspect ratio. Will the microstructural geometry dictate strength?

The purpose of the present work is to micromechanically examine the effect of the bio-inspired material architecture on its overall strength. For this purpose we use the “first principles” simulations. The latter means that we make no approximate assumptions concerning the mechanical behavior of the matrix or inclusions. We use the general continuum mechanics framework to describe the nonlinear constitutive response of soft matrix and hard platelets. It is crucial that we use an experimentally calibrated constitutive model for the natural rubber which includes a material failure description. The latter feature allows tracking the strength of the composite. Moreover, we combine the constitutive models with the high-fidelity generalized method of cells (HFGMC) which provides the micromechanical analysis of the periodic composite.

We find that the overall strength of the composite depends on the deformation and failure of rubber matrix in tension and shear. In addition, we find that the strength of the composite cannot exceed the strength of the matrix. The latter observation is noteworthy because it is qualitatively different from the previous experimental results with biocomposites [9,10,12,14,15] which show a dramatic (ten times) increase of the strength of the material as compared to the strengths of its constituents.

* Corresponding author.
E-mail address: cvolokh@technion.ac.il (K.Y. Volokh).

http://dx.doi.org/10.1016/j.ijmecsci.2017.06.054
Received 12 March 2017; Received in revised form 20 June 2017; Accepted 29 June 2017
Available online 4 July 2017
0020-7403/

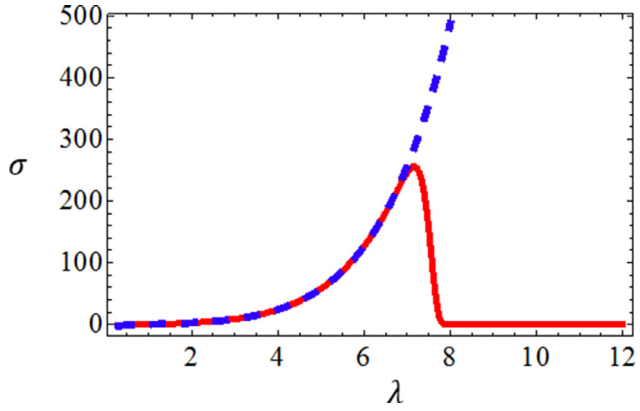

Fig. 1. True stress [MPa] - stretch in uniaxial tension of natural rubber: the dashed line is for the model without failure and the solid line is for the model with failure via the energy limiter.

2. Modeling

In this section we briefly introduce the multi-scale methodology for numerical analysis of the staggered composite. More detailed discussion can be found in [2]. As compared to the latter work we slightly modify the theoretical setting concerning the considered materials. The subsequent application of the methodology to the staggered bio-inspired composite is the main purpose of the computational micromechanical analysis.

2.1. Constitutive models

Soft material of the composite matrix is modeled by using elasticity with energy limiters [19,20,22,23]. According to this approach, an analytical expression of the strain energy is formulated in such way that it allows bounding the energy that can be stored and, consequently, dissipated by an elementary bulk volume. The idea of limiting the stored energy density is deeply rooted in physic because it enforces the average energy of particle bonds in continuum mechanics setting. For instance, two particles interact undergoing stages of repulsion, attraction, and separation. The latter stage begins at the limit point of the force-separation curve. This critical limit point happens due to the bond energy, which is the energy limiter on the scale of the particle interactions. For solids built of huge amounts of particles strain tensors are used to measure altering inter-particle distances and the strain energy function is used to represent the average potential of the particle interactions. Importantly, the limiters automatically bound stresses defined by the constitutive equations.

The strain energy function can be written in the following general form

$$\psi(\mathbf{F},\alpha) = \psi_{\mathrm{f}} - H(\alpha)\psi_{\mathrm{e}}(\mathbf{F}), \tag{1}$$

$$\psi_{\mathrm{f}} = \psi_{\mathrm{e}}(\mathbf{1}), \tag{2}$$

$$\|\mathbf{F}\| \to \infty \Rightarrow \psi_{\mathrm{e}}(\mathbf{F}) \to 0, \tag{3}$$

where ψ_{f} is the constant bulk *failure energy* and $\psi_{\mathrm{e}}(\mathbf{F})$ is the *elastic energy*; $H(\alpha)$ is the Heaviside step function, i.e. $H(z) = 0$ if $z < 0$ and $H(z) = 1$ otherwise; $\mathbf{1}$ is the identity tensor; $\mathbf{F} = \mathrm{Grad}\mathbf{x}(\mathbf{X})$ is the deformation gradient, in which $\mathbf{x}$ is the current position of a material point that was at $\mathbf{X}$ in the reference configuration; and $\|\mathbf{F}\| = \mathbf{F} : \mathbf{F} = \mathrm{tr}(\mathbf{F}^{\mathrm{T}}\mathbf{F})$ is a norm.

Switch parameter $\alpha \in (-\infty, 0]$ is defined by the evolution equation

$$\dot{\alpha} = -H\left(\epsilon - \frac{\psi_{\mathrm{e}}}{\psi_{\mathrm{f}}}\right), \quad \alpha(t=0) = 0, \tag{4}$$

where $0 < \epsilon \ll 1$ is a precision constant.

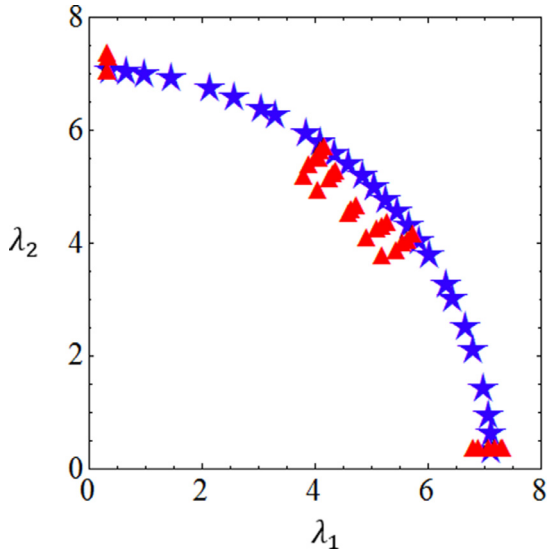

Fig. 2. Failure envelope for natural rubber in biaxial tension: theory (★) and tests (▲).

Presented constitutive law (1) means hyperelastic material behavior below ψ_{f}. After the limit the strain energy does not change providing the irreversibility of the process. We emphasize that α is not an internal variable like in the case of continuum damage theories. It is a switch parameter: if $\alpha = 0$ then the process is hyperelastic elastic; and if $\alpha < 0$ then material is irreversibly failed and energy dissipated.

Using the second law of thermodynamics and the Coleman-Noll procedure it is possible to obtain the constitutive law in the following form [23]

$$\mathbf{P} = -H(\alpha)\frac{\partial \psi_{\mathrm{e}}}{\partial \mathbf{F}}, \tag{5}$$

where $\mathbf{P}$ is the first Piola-Kirchhoff stress tensor.

The elastic energy is defined in general form following [20]

$$\psi_{\mathrm{e}}(\mathbf{F}) = \frac{\Phi}{m}\Gamma\left(\frac{1}{m}, \frac{W(\mathbf{F})^m}{\Phi^m}\right), \tag{6}$$

in which $\Gamma(s,x) = \int_x^\infty t^{s-1}e^{-t}dt$ is the upper incomplete gamma function; $W(\mathbf{F})$ is the stored energy of intact material; Φ is the energy limiter; and m is a parameter that shows how steep is the descending part of the stress-stretch curve.

The Yeoh model of natural rubber is used for the intact strain energy

$$W = \sum_{k=1}^{3} c_k(\mathbf{F} : \mathbf{F} - 3)^k, \ \det \mathbf{F} = 1, \tag{7}$$

where the constants were calibrated based on the results of experiments reported by [8]: $c_1 = 0.298$ MPa, $c_2 = 0.014$ MPa, $c_3 = 0.00016$ MPa.

By using these same data from [8] experiments, parameters $m = 10$ and $\Phi = 82.0$ MPa were fitted to the limit point at critical stretch $\lambda_{cr} = 7.12$. The true stress - stretch curve in uniaxial tension for the described above model with the energy limiter is presented in Fig. 1.

The described above calibration of the material model has been done for the case of uniaxial tension. In the case of biaxial tension with the varying biaxiality ratio the comparison of the tests [8] and the theory is encouraging as well. Fig. 2 presents the critical stretches in a thin sample of natural rubber undergoing tension with various biaxiality ratios. The critical stretches obey the condition of the singularity of the Hessian: $(\partial^2\psi/\partial\lambda_1^2)(\partial^2\psi/\partial\lambda_2^2) - (\partial^2\psi/\partial\lambda_1\partial\lambda_2)^2 = 0$. The latter condition defines the failure envelope in the stretch space. We note that the theory was calibrated in the uniaxial tension test and, expectedly, then slightly lower critical stretches in equibiaxial tension are observed due to the imperfection sensitivity of the tests.

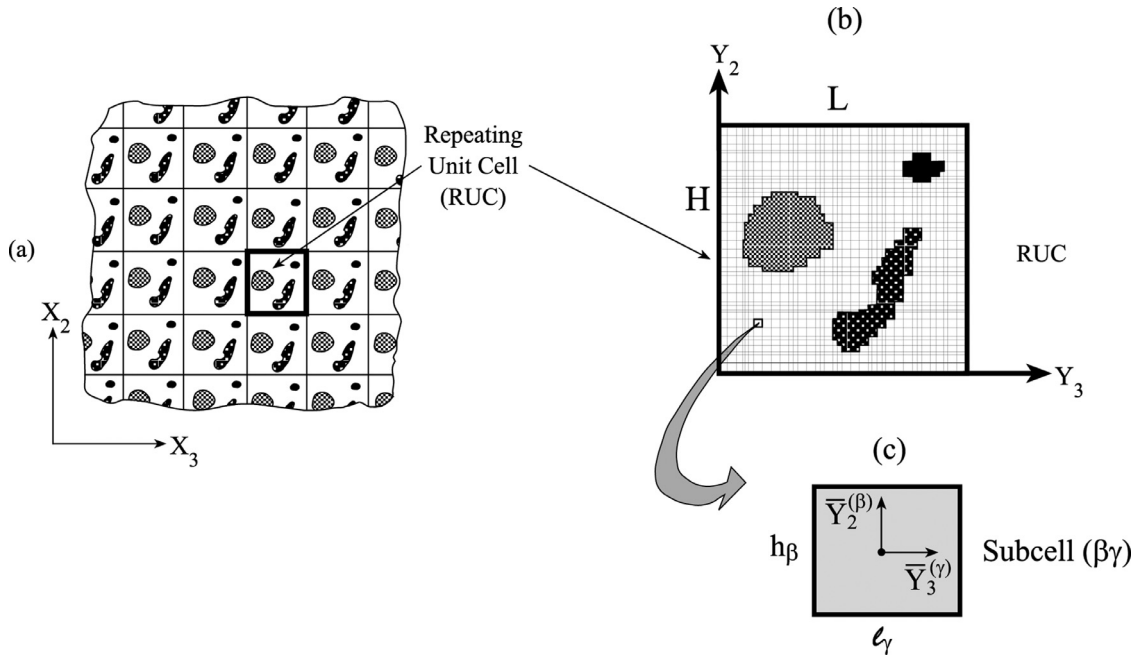

Fig. 3. (a) Doubly-periodic composite with respect to global reference coordinates $X_2 - X_3$; (b) The repeating unit cell with respect to local reference coordinates $Y_2 - Y_3$; (c) The sub-cell $(\beta\gamma)$ with local reference coordinates $\bar{Y}_2^{(\beta)}, \bar{Y}_3^{(\gamma)}$ (the origin is at the center).

Not only uniaxial and biaxial states of stresses and deformations are described well by the theory. Also, the case of three-dimensional hydrostatic tension was considered in [21] for the problem of an unstable cavity expansion - cavitation. The theoretical predictions were compared to the result of the "poker-chip" test done by [7]. Once again, the comparisons with the experimental data encourages the use of the methods of energy limiters.

We mention, finally, that more information on the use of the elasticity with energy limiters for rubberlike materials is presented in review by Volokh [22].

In addition to the application of the method of energy limiters to rubberlike materials the reader might be interested to learn the applications of the approach to the analysis of failure in hard brittle materials. For example, Volokh and Trapper [24] used the energy limiters approach to study the toughness of linear elastic materials.

Contrary to the description of the soft matrix the hard platelets are considered to deform without failure and the Kirchhoff – Saint-Venant material model is used with the strain energy function in the form

$$\psi = \frac{\Lambda}{2}(\mathrm{tr}\mathbf{E})^2 + \mu\mathbf{E} : \mathbf{E}, \tag{8}$$

in which $\mathbf{E} = (\mathbf{F}^{\mathrm{T}}\mathbf{F} - \mathbf{1})/2$ is the Green strain tensor and material are defined as follows: $\Lambda = 19.44$ GPa and $\mu = 29.17$ GPa that correspond to the Young modulus $E = 70$ GPa and Poisson ratio $\nu = 0.2$.

We intentionally use the Green strain tensor instead of the small strain tensor in order to suppresses the local influence of the rigid body motion in calculations. We also note that the particular magnitude of the Young modulus for the platelets is of minor importance because the matrix is much softer than the platelets and the latter ones can be reasonably interpreted as rigid inclusions.

2.2. Micromechanical analysis - the high-fidelity generalized method of cells (HFGMC)

The HFGMC micromechanics analysis for doubly-periodic composites at finite strains have been developed by [2]. So, we refer the interested reader to the mentioned work and we avoid the repetition of the details of the analysis. Nevertheless, we briefly review it as follows.

The micromechanical analysis utilizes a homogenization approach within which a periodic unit cell of the composite is used. A doubly-periodic composite, defined with respect to the initial global coordinates of the $X_2 - X_3$ plane, is shown in Fig. 3(a). Its repeating unit cell, defined with respect to the initial material coordinates $Y_2 - Y_3$, is shown in Fig. 3(b). The unit cell is decomposed into N_β and N_γ sub-cells in the Y_2 and Y_3 directions, respectively. Each sub-cell is labeled by the indices $(\beta\gamma)$ with $\beta = 1, \dots, N_\beta$ and $\gamma = 1, \dots, N_\gamma$ and it generally comprises various materials. The initial dimensions of sub-cell $(\beta\gamma)$ in directions Y_2 and Y_3 are denoted by h_β and l_γ, respectively, see Fig. 3(c). The local initial coordinate system $\bar{Y}_2^{(\beta)}, \bar{Y}_3^{(\gamma)}$ is introduced in each sub-cell whose origin is located at its center.

For the doubly periodic HFGMC, the incremental displacement vector $\triangle\mathbf{u}^{(\beta\gamma)}$ in sub-cell $(\beta\gamma)$ is presented via expansion into the second-order polynomials

$$\begin{aligned}\triangle\mathbf{u}^{(\beta\gamma)} = {} & \triangle\bar{\mathbf{F}}\mathbf{X} + \triangle\mathbf{W}_{(00)}^{(\beta\gamma)} + \bar{Y}_2^{(\beta)} \triangle \mathbf{W}_{(10)}^{(\beta\gamma)} + \bar{Y}_3^{(\gamma)} \triangle \mathbf{W}_{(01)}^{(\beta\gamma)} \\ & + \frac{1}{2}\left(3\bar{Y}_2^{(\beta)2} - \frac{h_\beta^2}{4}\right) \triangle \mathbf{W}_{(20)}^{(\beta\gamma)} + \frac{1}{2}\left(3\bar{Y}_3^{(\gamma)2} - \frac{l_\gamma^2}{4}\right) \triangle \mathbf{W}_{(02)}^{(\beta\gamma)},\end{aligned} \tag{9}$$

in which $\triangle\bar{\mathbf{F}}$ denotes the increment of the macroscopic deformation gradient and $\triangle\bar{\mathbf{F}}\mathbf{X}$ stands for the increment of the externally applied loading.

Coefficients $\triangle\mathbf{W}_{(mn)}^{(\beta\gamma)}$ are determined [2] from the equilibrium equations, inter-facial and periodic conditions, and the constitutive equations of the materials at finite strains.

The micromechanical analyses for the current loading increment provide the fourth-order instantaneous concentration tensor $\mathbb{A}^{(\beta\gamma)}$ that relates the local $\triangle\mathbf{F}^{(\beta\gamma)}$ and global $\triangle\bar{\mathbf{F}}$ deformation gradients

$$\triangle\mathbf{F}^{(\beta\gamma)} = \mathbb{A}^{(\beta\gamma)} : \triangle\bar{\mathbf{F}}. \tag{10}$$

For the hyperelastic strain energies defined above, it is possible to calculate the first Piola-Kirchhoff stress tensor $\triangle\mathbf{P}^{(\beta\gamma)}$ and the corresponding fourth-order tensor $\mathbb{R}^{(\beta\gamma)}$ for the sub-cell as follows

$$\triangle\mathbf{P}^{(\beta\gamma)} = \mathbb{R}^{(\beta\gamma)} : \triangle\bar{\mathbf{F}}. \tag{11}$$

Then, the incremental average stress is obtained as

$$\triangle\bar{\mathbf{P}} = \frac{1}{HL}\sum_{\beta=1}^{N_\beta}\sum_{\gamma=1}^{N_\gamma} h_\beta l_\gamma \triangle \mathbf{P}^{(\beta\gamma)}. \tag{12}$$

Substituting the incremental constitutive Eq. (11) for $\triangle\mathbf{P}^{(\beta\gamma)}$ and using (10) we obtain the global incremental constitutive equation of the composite

$$\triangle\bar{\mathbf{P}} = \mathbb{R}^* : \triangle\bar{\mathbf{F}}, \tag{13}$$

where

$$\mathbb{R}^* = \frac{1}{HL}\sum_{\beta=1}^{N_\beta}\sum_{\gamma=1}^{N_\gamma} h_\beta l_\gamma \mathbb{R}^{(\beta\gamma)} : \mathbb{A}^{(\beta\gamma)} \tag{14}$$

is the effective instantaneous fourth order tangent tensor

In summary, the HFGMC micromechanical analysis of the doubly-periodic composites establishes the macroscopic constitutive equations governing behavior of the soft matrix that can fail and the rigid platelets without failure. The loss of static stability in a sub-cell, which is filled by a hyperelastic material (with the energy limiter), affects the composite response and indicates the onset of the global failure in the composite - its *strength*.

The details and the reliability of the finite strain HFGMC formulation for doubly-periodic soft composites can be found in [2], in which a radially stretched hollow cylinder was studied. Analytical and finite-difference solutions were developed for various hyperelastic materials with substantially different behavior. These solutions were compared to the HFGMC-based analyses and perfect agreements were observed.

3. Simulation results

In this section we present results of micromechanical simulations of a bio-inspired composite in uniaxial tension. Our software is an in-house one and it is based on the detailed description of the micromechanical analysis given by Aboudi et al. [1]. For the simulation we use the approaches discussed above which include a failure description of soft hyperelastic matrix and a micromechanical account of the hard inclusions.

Four cases of composites are examined - Fig. 4.

Case 1 is an ideally connected composite. The soft matrix and hard platelets are described by the constitutive models discussed in Section 2.1.

Case 2 is a partially cracked composite. The cracks are introduced via the absence of the connecting soft matrix at some (short) edges of the platelets. In the case of the uniaxial tension these cracks are in Mode 1.

Case 3 is fully cracked, in Mode 1, composite where all short edges of the platelets are free of soft matrix.

Case 4 is fully cracked in Mode 1 and partially cracked in Mode 2.

The repeating unit cells corresponding to all four cases of the composite are shown in Fig. 5. The dimensionless length parameters are: $l = 200$, $d = 20$, $b = 2$. This choice of the length parameters corresponds to the following amount of hard inclusions in a unit cell

$$V_{\text{inc}} = \frac{ld}{(l+b)(b+d)}100\% = 90\%.$$

It should be noted that $l/d = 10$ is consistent with the platelet ratio observed in biocomposites [11].

We emphasize that the constitutive description of the soft matrix includes failure – the limit point in Fig. 1. When the limit point is passed locally during loading then static equilibrium is lost and failure initiates, localizes, and propagates through the material. In the present study (and using the approaches described above) we only track the initiation of failure which is the material strength in uniaxial tension. Thus, we simulate the whole quasi-static loading path including the failure onset. Four simulation cases are presented in Fig. 6.

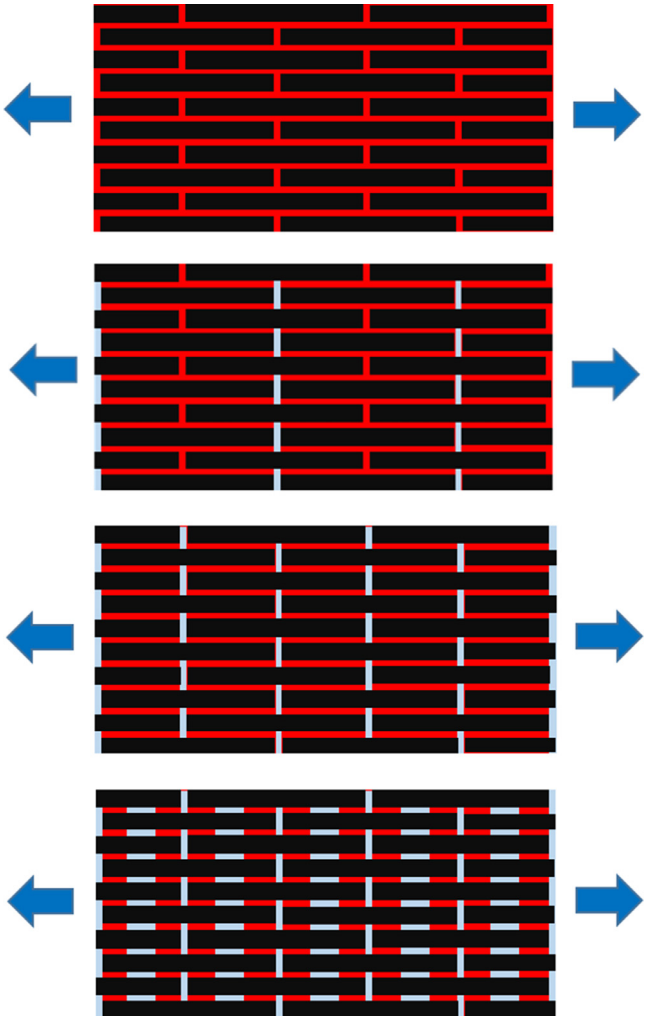

Fig. 4. Bio-inspired composites: platelets (black); soft matrix (red); cracks (light blue). From the top to the bottom: Case 1 - fully connected; Case 2 - partial Mode 1 cracks; Case 3 - full Mode 1 cracks; Case 4 - full Mode 1 and partial Mode 2 cracks. (For interpretation of the references to color in this figure legend, the reader is referred to the web version of this article.)

Fig. 7 presents shots of the energy maps during the loading of all four cases under consideration. The energy maps indicate areas with higher energy where the failure initiation is expected.

Intuitively, the reader might expect that the stiffness of the composite declines with the increasing number of cracks. That is true, indeed. However, the alterations of the onset of failure shown in Fig. 6 could hardly be expected. The ideally bonded composite has the critical stress of the onset of failure close to ~40 MPa. It can be seen from the top of Fig. 7 that the highest energy consumption occurs in the soft matrix along the short edges of the platelets. These are the areas where failure initiates. In case 2 where some cracks in these areas are induced the remaining parts of soft matrix at the short edges of the platelets bear the most energy. Since less soft material is involved in the process, the critical stress of the onset of failure expectedly decreases to ~25 MPa.

The areas of soft matrix near the short edges of the platelets are definitely the weakest links of the composite, in which failure occurs. Inducing cracks in these areas it is possible to get rid of the weakest links and significantly increase the critical stress of the onset of failure to ~150 MPa. It is not only the critical stress but also the critical stretch increases from 1.04 to 1.14. It is truly remarkable that by adding cracks and, contrary to intuition, it is possible to increase the point of the critical stress of the onset of failure of the composite. In case 3, the soft matrix areas along the long edges of the platelets bear the load.

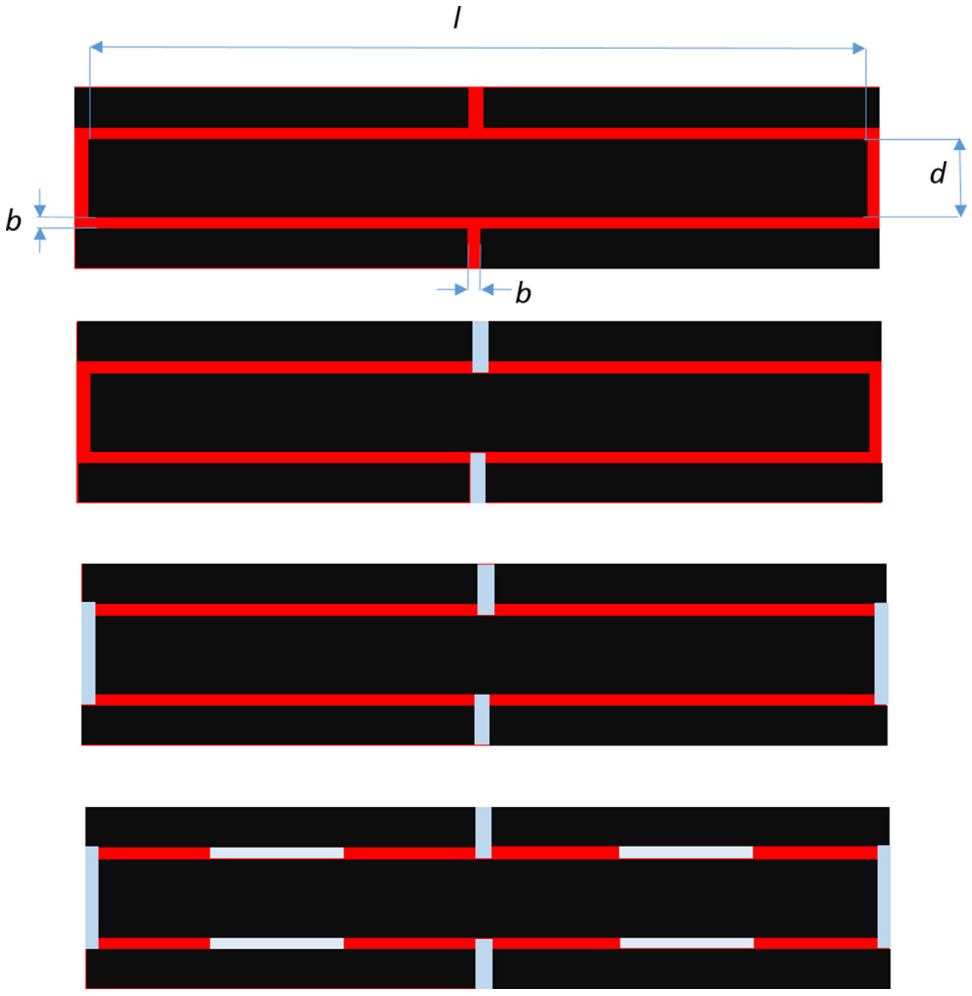

Fig. 5. Repeating unit cells for four cases of the composite.

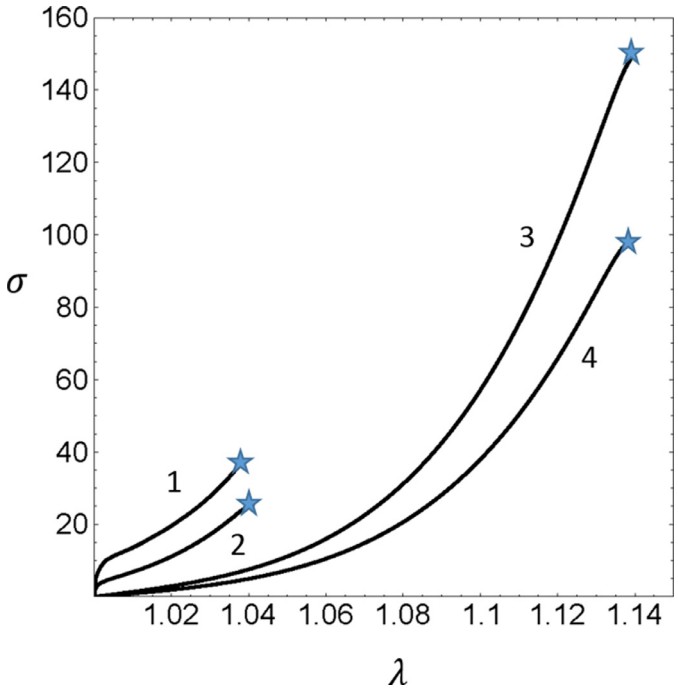

Fig. 6. Cauchy stress [MPa] versus stretch in uniaxial tension for four cases of the composite (90% reinforcement). Stars designate the onset of failure - strength.

Introducing further cracks in the shear regions of the matrix we reduce the critical stress of the onset of failure of the composite to ~100 MPa because less material bears load - Fig. 6. Nevertheless, the character of the deformation does not change qualitatively.

In addition to the composite with the 90% amount of hard inclusions we consider a similar composite with 80% of hard inclusions by defining the geometrical parameters as follows: $l = 188$, $d = 18$, $b = 4$. The stress-stretch curves for these same four cases of the composite (Fig. 4) are generated and shown in Fig. 8.

Comparing Figs. 6 and 8 it is interesting to note, first of all, that the amount of stretch up to all failure points increased. In cases 1 and 2 the critical stretch for 80% is ~1.1 as compared with ~1.04 for 90% reinforcement. In cases 3 and 4 the critical stretch for 80% is ~1.28 as compared with ~1.14 for 90% reinforcement. Obviously, the larger amount of soft matrix allowed larger deformations. The latter also means that the stiffness of the composite decreased as expected. The situation with the critical stress of the onset of failure is subtler. In the cases 1 and 2 where the critical stress is caused by tension of the matrix material at the short edges of the platelets we observe some increase of it for 80% reinforcement as compared with 90%. The latter increase can probably be explained by the fact that the deformation state in these thin areas starts changing from pure shear and even hydrostatic tension to the state of uniaxial tension, which can accommodate higher stresses and, consequently, the higher critical stress of the onset of failure. In cases 3 and 4 where the critical stress is caused by shear of the matrix material at the long edges of the platelets we observe some decrease of it for 80% reinforcement as compared with 90%. The latter decrease can probably

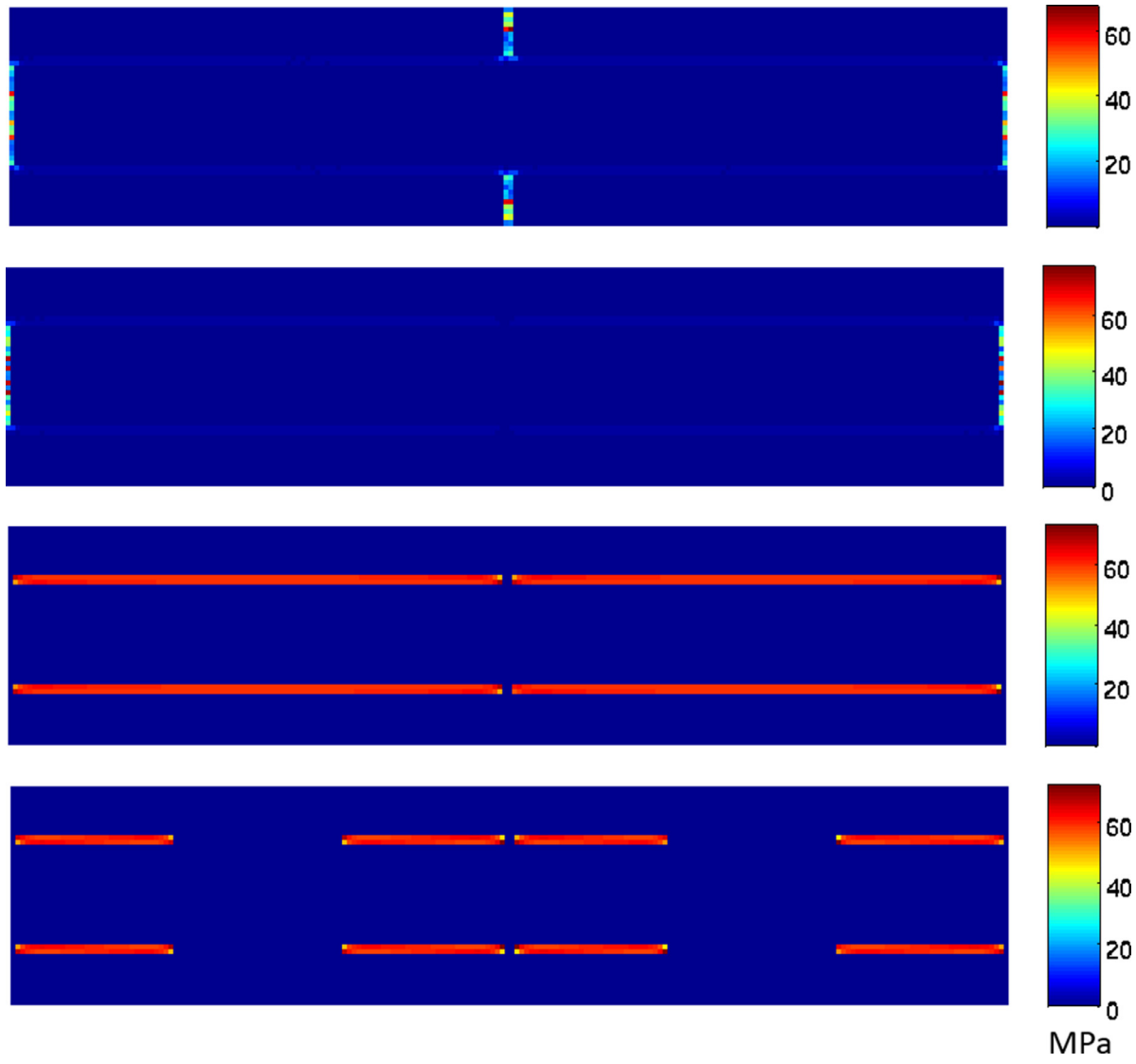

Fig. 7. Strain energy maps for the composite cases 1–4 from the top to the bottom respectively.

be explained by the fact that the overall strain energy is accommodated by larger deformation in the case of the larger amount of soft material and, as a result of that, the strength slightly goes down.

Finally we note that in all considered cases the overall critical stress of the composite did not exceed the strength of the soft matrix ~250 MPa.

Remark on strength. In the analysis above we discussed the critical stress of the onset of failure. We intentionally did not use the word "strength" because its meaning can be arguable in view of the reported simulations. Now, we can define the strength as the *maximum critical stress* that appears in Figs. 6 and 8. Indeed, material can bear more load with mode 1 cracks. The material strength is defined by the critical state when soft matrix is in shear.

4. Experiments

In this section we report the experimental studies that validate the theoretically predicted deformation modes ***qualitatively*** - the reader is also addressed to the supplementary material with the taped experiment. Unfortunately, we are technically unable to reproduce (print) the natural rubber matrix and keep the aspect ratio of platelets in experiments. We use a different (rate-sensitive) soft material instead of natural rubber.

The sample corresponds to case 1 composite in the numerical simulations. It was fabricated by using a multi-material Polyjet technique with a help of the 3D-printer Objet Connex 260. The chosen geometrical parameters were $l = 17.50$ mm, $d = 3.50$ mm, $b = 0.7$ mm and the total length, width and thickness of the samples were equal to 110 mm, 42 mm and 4 mm, respectively. Through the survey of the mechanical properties of available materials, we identified suitable combinations of constituents for stiff and soft constituents. In particular, the stiff platelets were printed in rigid VeroWhite polymer (further referred as VW), while the soft interfaces were printed in soft hyperelastic digital material (further referred as DM50). Through the mechanical testing of the homogeneous VW and DM50 materials, determine the materials constants for both polymers. VW material can be defined as linear elastic material with Young's modulus of $E = 1.8$ GPa and Poisson's ratio $\nu = 0.42$. The interface digital material DM50 can be considered as incompressible hyperelastic material with the shear modulus of $\mu = 0.41$ MPa and critical stretch ratio of 1.62. To study the mechanical properties, the printed bio-inspired composites were subjected to uniaxial tension by using a universal testing machine Shimadzu EZ-LX. In order to diminish a possible rate-dependent behavior of the interface DM50 materials [18], the uniaxial tension was performed at a slow strain rate of 10^{-4} 1/s.

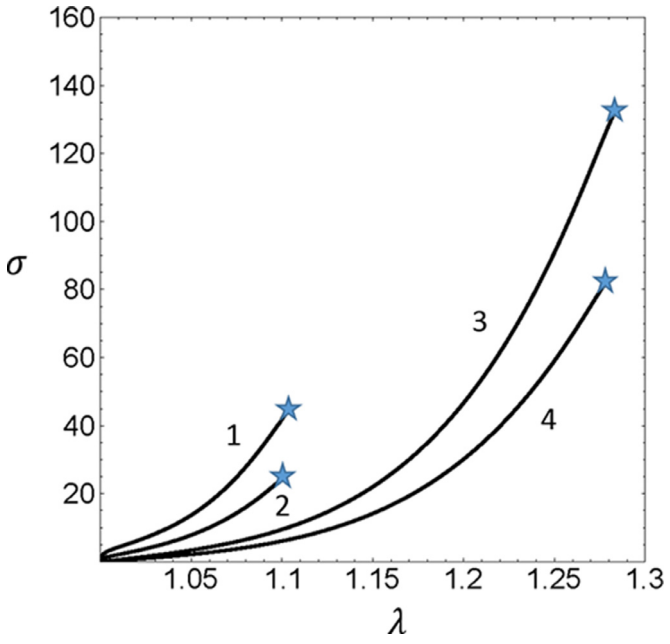

Fig. 8. Cauchy stress [MPa] versus stretch in uniaxial tension for four cases of the composite (80% reinforcement). Stars designate the onset of failure.

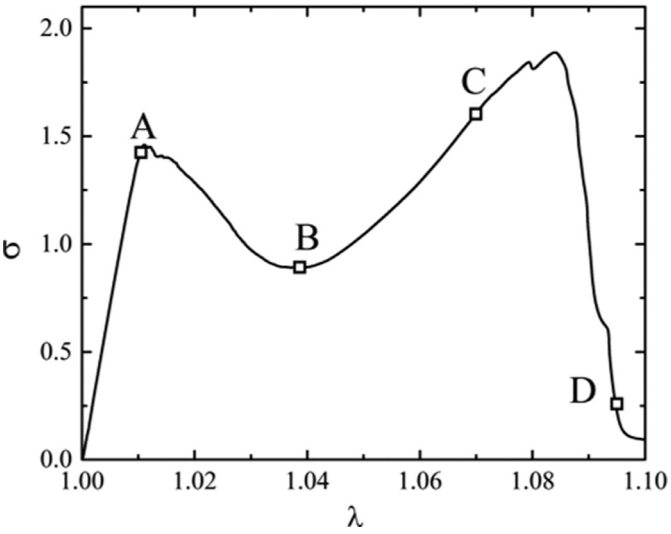

Fig. 9. Experimental stress [MPa]-stretch curve.

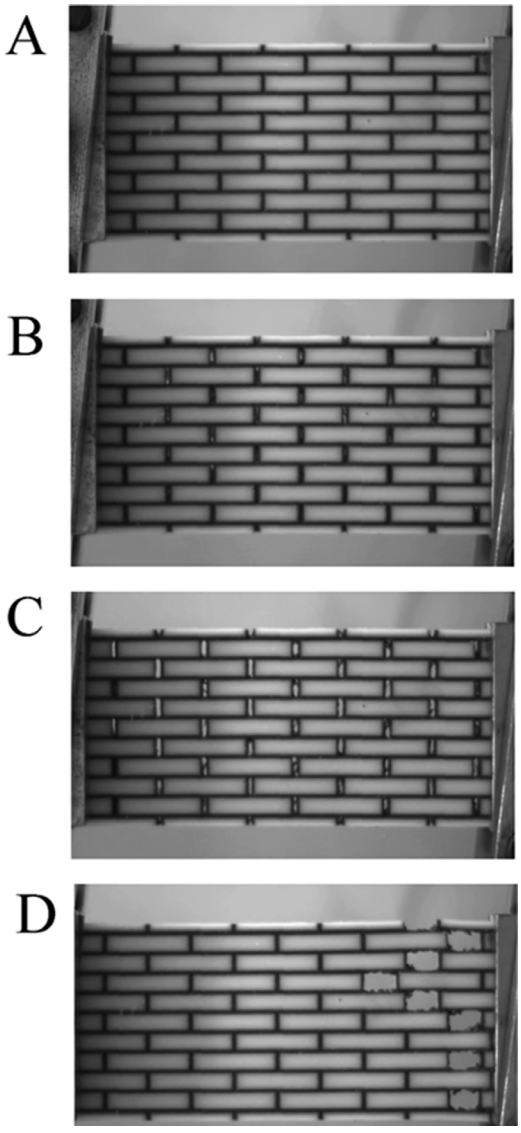

Fig. 10. Snapshots of the experiment tape at points A, B, C, D.

Fig. 9 shows the stress-strain curve, obtained for the case 1 composite, subjected to uniaxial tension. Fig. 10 shows the snapshots of the experiment tape at points A, B, C, D shown in Fig. 9.

One may see that after reaching the critical level of loading - point A ($\lambda = 1.01$), the soft material at the short platelet edges fail. This leads to a significant drop in stress level during the following loading up to point B ($\lambda = 1.04$). Then the shear deformation in the soft matrix along the lengthy edges of platelets dominates until approximately point C ($\lambda = 1.08$) soon after which the ultimate stress - strength - is reached and material starts disintegrating as at point D. This observation supports the numerically predicted phenomena - Figs. 6 and 8 - showing that the catastrophic failure originates in the soft interfacial phase, and it has a significant influence on the overall strength of the composite.

5. Discussion

This theoretical study on the influence of the staggered alignment of hard platelets with high aspect ratio on the overall *strength* of bio-inspired composites appears to be the first report where continuum mechanics formulation incorporating a failure description and the high-fidelity generalized method of cells were combined. Previous studies considered primarily stiffness and (mainly qualitatively) fracture toughness of such composites (e.g. [13,27]).

Consideration of strength in the present work became possible due to the novel modeling technique used in this study. First, hyperelasticity with energy limiters was applied to describe deformation and failure of soft matrix material and the experimentally calibrated constitutive law for the natural rubber vulcanizate was utilized. Second, the finite strain high-fidelity generalized method of cells (HFGMC) was used for the micromechanical modeling of the soft matrix–hard platelet composite. Combination of these techniques allowed us to perform full-scale micromechanical simulations of uniaxial tension in bio-inspired composite. We generated stress-stretch curves including the point of the onset of mechanical failure. The stress-stretch curves were generated for 8 different cases of the composite material with various amounts of hard inclusions: 80% and 90%; and cracks: perfect bonding; partial Mode 1 cracking; full Mode 1 cracking; full Mode 1 cracking and partial Mode 2 cracking. In addition, the maps of the strain energy were generated which indicated the locations of the possible occurrence of failure that might affect the overall strength.

Our results show that larger amounts of hard inclusions lead to the stiffer composites. That is in line with the similar findings for composite materials in general and biocomposites, in particular. While the stiffening effect of the embedded hard inclusions is well known in the literature, the study of the strength (rather than stiffness) alterations is quite novel. Such lack of symmetry in results on stiffness and strength is not surprising: it occurs because the traditional constitutive descriptions of materials do not incorporate failure and, therefore, strength cannot be analyzed. That is not our case. We included a material failure description in the theoretical model for soft matrix and we could study the strength of the bio-inspired composite.

Our simulations of the bio-inspired composites provided various outcomes. We found, for example, that the soft matrix material placed between the short edges was the weakest link of the composite with the high strain energy density. These were the areas where failure initiated and critical stress was reached. Amazingly, by deleting soft material or introducing pre-existing cracks in these dangerous areas it was possible to significantly increase (~4 times) the critical stress of the composite. Such finding might seem contrary to intuition at first glance. However, the pre-existing cracks actually relieved the stress and strain concentrators providing greater material resistance. The main load bearing area of the matrix became the region connecting long edges of the platelets. This region was predominantly in the state of shear. The failure of soft matrix in shear was responsible for the *overall strength* of the composite. Importantly, the overall strength did not exceed the strength of the matrix material in the uniaxial tension.

Our findings emphasize that material stiffness and strength are not related. The latter fact is not always appreciated. The strength of a composite is significantly affected by the locally nonuniform state of deformation. Hard particles can create the strain and stress concentrations increasing the probability of the local material failure.

We note that the natural rubber vulcanizate is not as rate-sensitive as the material used in 3D printing. Unfortunately, we cannot fabricate the composite materials with rate insensitive behavior. Nevertheless, we observe that the obtained results are similar qualitatively. This suggests that our conclusions may be applied for composites with rate-sensitive constituents. Thus, potentially it allows us to make similar predictions for a more general class of materials.

We additionally emphasize that we deal with bio-inspired rather than with real bio- composites. The strength mechanism in real biocomposites remains unrevealed. The main message of our work is that the simple “architectural hypothesis” concerning the strength of bio-inspired composites may not fully elucidate the phenomenon. Thus, our analytical, numerical, and experimental results suggest that the outstanding strength of biocomposites may not be just due to their geometrical composition but, rather, due to new bonds created at the nanoscale lengths. Actually, biocomposites might not be composites in the regular sense but, rather, they might be essentially new materials with special new properties. Arguably, the methods of the classical continuum mechanics (usually used in the literature) should incorporate the information from these different length-scales for proper elucidation of the remarkable mechanical properties of biocomposites.

Supplementary material

Supplementary material associated with this article can be found, in the online version, at 10.1016/j.ijmecsci.2017.06.054

Acknowledgment

Fruitful discussions with Professor Herzl Chai are gratefully appreciated. In addition, KV and JA acknowledge the support from the Israel Science Foundation, ISF-198/15. SR acknowledges the support from the Israel Science Foundation through the projects 1550/15 and 1973/15. SR gratefully acknowledges the support of Taub Foundation through the Horev Fellowship – Leaders in Science and Technology. VS acknowledges the support provided by the Russian Science Foundation through project 15-11-10000.

References

[1] Aboudi J, Arnold SM, Bednarcyk B. Micromechanics of composite materials: a generalized multiscale analysis approach. Oxford: Elsevier; 2013.
[2] Aboudi J, Volokh KY. Failure prediction of unidirectional composites undergoing large deformations. J Appl Mech 2015;82:071004.
[3] Barthelat F, Rim JE, Espinosa HD. A review on the structure and mechanical properties of Mollusk shells – perspectives on synthetic biomimetic materials. Applied scanning probe methods XIII: biomimetics and industrial applications. Bhushan B, Fuchs H, editors. Berlin: Springer; 2009.
[4] Chai H. On the mechanical properties of tooth enamel under spherical indentation. Acta Biomater 2014;10:4852–60.
[5] Gao H, Ji B. Modeling fracture in nanomaterials via a virtual internal bond method. Eng Fract Mech 2003;70:1777–91.
[6] Gao H, Ji B, Jager IL, Arzt E, Fratzl P. Materials become insensitive to flaws at nanoscale: lessons from nature. PNAS 2003;100:5597–600.
[7] Gent AN, Lindley PB. Internal rupture of bonded rubber cylinders in tension. Proc Roy Soc A 1959;2:195–205.
[8] Hamdi A, Nait Abdelaziz M, Ait Hocine N, Heuillet P, Benseddiq N. A fracture criterion of rubber-like materials under plane stress conditions. Polym Test 2006;25:994–1005.
[9] Jackson AP, Vincent JFV, Turner RM. The mechanical design of nacre. Proc R Soc London B 1988;234:415–40.
[10] Jager I, Fratzl P. Mineralized collagen fibrils: a mechanical model with a staggered arrangement of mineral particles. Biophys J 2000;79:1737–46.
[11] Ji B, Gao H. Mechanical properties of nanostructure of biological materials. J Mech Phys Solids 2004;52:1963–90.
[12] Kamat S, Su X, Ballarini R, Heuer H. Structural basis for the fracture toughness of the shell of the conch Strombus Gigas. Nature 2000;405:1036–40.
[13] Lei HF, Zhang ZQ, Liu B. Effect of fiber arrangement on mechanical properties of short fiber reinforced composites. Compos Sci Technol 2012;72:506–14.
[14] Menig R, Meyers MH, Meyers MA, Vecchio KS. Quasi-static and dynamic mechanical response of Haliotis Rufescens (abalone) shells. Acta Mater 2000;48:2383–98.
[15] Norman TL, Vashishtht D, Burr DB. Fracture toughness of human bone under tension. J Biomech 1995;28:309–20.
[16] Rudykh S, Boyce MC. Analysis of elasmoid fish imbricated layered scale-tissue systems and their bio-inspired analogues at finite strains and bending. IMA J Appl Math 2014;79:830–47.
[17] Rudykh S, Ortiz C, Boyce MC. Flexibility and protection by design: imbricated hybrid microstructures of bio-inspired armor. Soft Matter 2015;11:2547–54.
[18] Slesarenko V, Rudykh S. Harnessing viscoelasticity and instabilities for tuning wavy patterns in soft layered composites. Soft Matter 2016;12:3677–82.
[19] Volokh KY. Hyperelasticity with softening for modeling materials failure. J Mech Phys Solids 2007;55:2237–64.
[20] Volokh KY. On modeling failure of rubberlike materials. Mech Res Commun 2010;37:684–9.
[21] Volokh KY. Cavitation instability in rubber. Int J Appl Mech 2011;3:29311.
[22] Volokh KY. Review of the energy limiters approach to modeling failure of rubber. Rubber Chem Technol 2013;86:470–87.
[23] Volokh KY. On irreversibility and dissipation in hyperelasticity with softening. J Appl Mech 2014;81:074501.
[24] Volokh KY, Trapper P. Fracture toughness from the standpoint of softening hyperelasticity. J Mech Phys Solids 2008;56:2459–72.
[25] Wegst UGK, Bai H, Saiz E, Tomsia AP, Ritchie RO. Bioinspired structural materials. Nature Mater 2014:4089.
[26] Xie Z-H, Swain MV, Swadener G, Munroe P, Hoffman M. Effect of microstructure upon elastic behaviour of human tooth enamel. J Biomech 2009;42:1075–80.
[27] Zhang ZQ, Liu B, Huang Y, Hwang KC, Gao HJ. Mechanical properties of unidirectional nanocomposites with non-uniformly or randomly staggered platelet distribution. J Mech Phys Solids 2010;58:1646–60.